International Journal of Automation and Computing 9(4), August 2012, 342-351
DOI: 10.1007/s11633-012-0654-0

Integrated Relative Position and Attitude Control of Spacecraft in Proximity Operation Missions

Feng Zhang Guang-Ren Duan

Center for Control Theory and Guidance Technology, Harbin Institute of Technology, Harbin 150001, China

Abstract: This paper addresses an integrated relative position and attitude control strategy for a pursuer spacecraft flying to a space target in proximity operation missions. Relative translation and rotation dynamics are both presented, and further integratedly considered due to mutual couplings, which results in a six degrees-of-freedom (6-DOF) control system. In order to simultaneously achieve relative position and attitude requirements, an adaptive backstepping control law is designed, where a command filter is introduced to overcome "explosion of terms". Within the Lyapunov framework, the proposed controller is proved to ensure the ultimate boundedness of relative position and attitude signals, in the presence of external disturbances and unknown system parameters. Numerical simulation demonstrates the effect of the designed control law.

Keywords: Spacecraft, integrated translation and rotation control, adaptive backstepping, command filter, ultimate boundedness.

1 Introduction

By virtue of growing space activities worldwide, autonomous spacecraft proximity operations have received increasing attention in recent years. Especially, their great application prospects and importance have been gradually shown in missions including space debris removing, in-orbit satellite maintenance, spatial refueling, spacecraft formation flying, and space station installation. Furthermore, several programs have been brought forward and even developed as technology demonstrations, such as NASA′s DART program[1], SSC′s Prisma project[2], and Orbital Servicing Limited′s CX-OLEV[3]. It is noticeable that, to ensure these missions′ success, autonomous rendezvous with precise position and attitude control is the key technology[4].

The background of this paper accounts for the problem of forcing an active spacecraft, namely pursuer, to approach a target spacecraft in proximity, and simultaneously enabling the attitude of pursuer synchronize with the target.

In view of space operations, the kinematics and dynamics of the spacecraft always perform highly nonlinear. Early studies usually separately considered the translation and rotation maneuvers of a spacecraft[5, 6]. However, the orbital and attitude subsystems are mutually coupled, which is mainly due to the dependence of the thrust orientation for translation control on the spacecraft attitude and the thruster configuration. Therefore, different from the separated control strategy, the proximity operations in consideration fiercely necessitate a systematic precise control strategy for 6-DOF coupled position and attitude motion of a maneuverable pursuer spacecraft. This challenging problem has been increasingly focused on in recent years[7−13]. Reference [7] proposed an adaptive nonlinear tracking control law to ensure the global asymptotic convergence of the relative translation and attitude position tracking errors. Using the same model, an output feedback tracking control to achieve the same goal was put forward in [8]. A nonlinear integrated position and attitude suboptimal control method, namely θ-D technique, was presented to cope with spacecraft proximity operations, including space debris capture[9] and tumbling target approach[10, 11]. Reference [12] designed a globally stable chattering free sliding mode robust controller to enable both position and attitude tracking error converge to equilibrium, where a thruster layout was considered. Reference [13] utilized three nonlinear state feedback controllers, involving passivity-based PD-plus controller, sliding surface controller, and integrator backstepping controller, to solve the problem of tracking relative 6-DOF motion in a leader-follower spacecraft formation.

Owing to the recursive use of Lyapunov functions, integrator backstepping is regarded as a powerful nonlinear control method leading to a wide application[13−15]. Nevertheless, it is important to note that the standard backstepping technique easily suffers from "explosion of terms" caused by repeated differentiations of desired virtual controllers[16−20]. To surmount this flaw, a dynamic surface control (DSC) technique was proposed and developed[16−19], where a first order filtering of the synthesized desired virtual control law was introduced at each step of the backstepping design procedure. Reference [20] came up with a command filtered backstepping method, where a second-order filtering of the command signal was used to obviate the need for the analytic computation of the desired virtual control and its differentiations. Moreover, the rigorous analysis of the command filter on closed-loop stability was stated with Tikhonov′s theorem.

In this paper, based on the 6-DOF translational and rotational dynamics of the pursuer spacecraft relative to the target spacecraft[21], taking thruster layout into account, an integrated position and attitude control strategy is designed by using adaptive backstepping technique and singular perturbation theory, where a command filter[20] is used to overcome the "explosion of terms". It follows that, by using Lyapunov theorem[22, 23], the proposed control law guarantees the ultimate boundedness of the relative position and

Manuscript received December 26, 2010; revised October 9, 2011
This work was supported by Innovative Team Program of the National Natural Science Foundation of China (No. 61021002).

attitude signals, in spite of unknown parameters and external disturbances; moreover, the corresponding bounds can be made arbitrarily small by adjusting parameters appropriately. A numerical simulation illustrates the effect of the designed control law.

The rest of this paper is organized as follows. In Section 2, the translational and rotational coupled dynamics of the spacecraft are stated. Then, an integrated translational and rotational adaptive backstepping control law is developed for the coupled system in Section 3. Next, numerical simulation results applying the proposed control law to a scenario of forcing a spacecraft to pursue a space target are presented in Section 4. At last, Section 5 draws the conclusions.

2 Problem formulation

In the scope of this study, a pursuer spacecraft is considered to approach a space target in proximity with simultaneous attitude maneuvering. Hence, to precisely control the relative position and attitude of two spacecraft, the relative translational and rotational dynamics modeling is necessary. To this end, several frames are described first, and then based on [21], the relative position and attitude coupled dynamics are formulated.

As shown in Fig. 1, the inertial frame is represented by the standard earth-centred inertial (ECI) frame $\mathcal{F}_i$. Additionally, the orbit frame is the standard local vertical/local horizontal (LVLH) frame $\mathcal{F}_t$ centered on the target with the basis vectors of the frame being defined as $\boldsymbol{e}_r = \boldsymbol{r}_t/r_t, \boldsymbol{e}_\theta = \boldsymbol{e}_h \times \boldsymbol{e}_r, \boldsymbol{e}_h = \boldsymbol{h}/h$, where $\boldsymbol{h} = \boldsymbol{r}_t \times \dot{\boldsymbol{r}}_t$ is the angular momentum vector of the target motion orbit and $h = \|\boldsymbol{h}\|$. The relative position vector between two spacecraft is denoted by

$$\boldsymbol{p} = \boldsymbol{r}_p - \boldsymbol{r}_t = x\boldsymbol{e}_r + y\boldsymbol{e}_\theta + z\boldsymbol{e}_h. \tag{1}$$

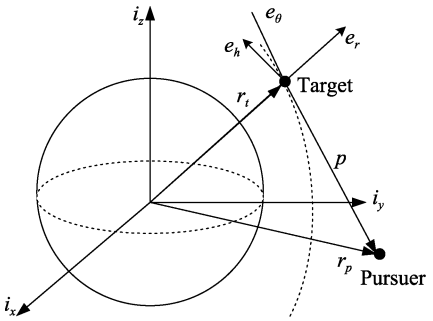

Fig. 1 Coordinate frames

Moreover, the body frames of the pursuer and target, $\mathcal{F}_{pb}$ and $\mathcal{F}_{tb}$, are also respectively formulated with origin in the corresponding center of mass and unit vectors coincide with their principal axes of inertia.

According to the basic equation of the two-body problem, the nonlinear relative dynamics can be represented in frame $\mathcal{F}_t$ as

$$m_p\ddot{\boldsymbol{p}} + \boldsymbol{C}_t(\dot{\gamma})\dot{\boldsymbol{p}} + \boldsymbol{D}_t(\dot{\gamma}, \ddot{\gamma}, r_p)\boldsymbol{p} + \boldsymbol{n}_t(\boldsymbol{r}_p, \boldsymbol{r}_t) = \boldsymbol{F}_a + \boldsymbol{F}_d \tag{2}$$

where m_p is the mass of the pursuer; γ is the true anomaly of the target; $\boldsymbol{F}_a \in \mathbf{R}^3$ is control force vector, while $\boldsymbol{F}_d$ denotes disturbance forces; $\boldsymbol{C}_t(\dot{\gamma})$, $\boldsymbol{D}_t(\dot{\gamma}, \ddot{\gamma}, r_p)$, $\boldsymbol{n}_t(r_p, r_t)$ yield

$$\boldsymbol{C}_t(\dot{\gamma}) = 2m_p\dot{\gamma}\begin{bmatrix} 0 & -1 & 0 \\ 1 & 0 & 0 \\ 0 & 0 & 0 \end{bmatrix} \tag{3}$$

$$\boldsymbol{D}_t(\dot{\gamma}, \ddot{\gamma}, r_p) = m_p\begin{bmatrix} \frac{\mu}{r_p^3} - \dot{\gamma}^2 & -\ddot{\gamma} & 0 \\ \ddot{\gamma} & \frac{\mu}{r_p^3} - \dot{\gamma}^2 & 0 \\ 0 & 0 & \frac{\mu}{r_p^3} \end{bmatrix} \tag{4}$$

$$\boldsymbol{n}_t(r_p, r_t) = m_p\mu\begin{bmatrix} \frac{r_t}{r_p^3} - \frac{1}{r_t^2} & 0 & 0 \end{bmatrix}^{\mathrm{T}}. \tag{5}$$

On the other hand, the relative attitude kinematics can be expressed as

$$\dot{\boldsymbol{q}} = \boldsymbol{T}(\boldsymbol{q})\omega \tag{6}$$

where $\boldsymbol{q}^{\mathrm{T}} = \begin{bmatrix} q_0 & \boldsymbol{q}_v^{\mathrm{T}} \end{bmatrix}$ is the unit quaternion representing the relative attitude of two spacecraft, satisfying the constraint[24]

$$q_0^2 + \boldsymbol{q}_v^{\mathrm{T}}\boldsymbol{q}_v = 1 \tag{7}$$

with $q_0 \in \mathbf{R}$, $\boldsymbol{q}_v \in \mathbf{R}^3$, and

$$\boldsymbol{T}(\boldsymbol{q}) = \frac{1}{2}\begin{bmatrix} -\boldsymbol{q}_v^{\mathrm{T}} \\ q_0\boldsymbol{I} + \boldsymbol{S}(\boldsymbol{q}_v) \end{bmatrix},\ \boldsymbol{T}(\boldsymbol{q})^{\mathrm{T}}\boldsymbol{T}(\boldsymbol{q}) = \frac{1}{4} \tag{8}$$

where $\boldsymbol{S}(\boldsymbol{q}_v) = \boldsymbol{q}_v\times$ is the cross product operator.

The relative angular velocity between frames $\mathcal{F}_{pb}$ and $\mathcal{F}_{tb}$ expressed in frame $\mathcal{F}_{pb}$ is governed by

$$\omega = \omega_{i,pb}^{pb} - \boldsymbol{R}_{tb}^{pb}\omega_{i,tb}^{tb} \tag{9}$$

where $\omega_{i,pb}^{pb}$ denotes the inertial angular velocity of frame $\mathcal{F}_{pb}$ expressed in frame $\mathcal{F}_{pb}$; while $\omega_{i,tb}^{tb}$ denotes that of frame $\mathcal{F}_{tb}$ expressed in frame $\mathcal{F}_{tb}$. $\boldsymbol{R}_{tb}^{pb}$ represents the transformation matrix from frame $\mathcal{F}_{tb}$ to $\mathcal{F}_{pb}$ and yields

$$\boldsymbol{R}_{tb}^{pb} = (q_0^2 - \boldsymbol{q}_v^{\mathrm{T}}\boldsymbol{q}_v)\boldsymbol{I} + 2\boldsymbol{q}_v\boldsymbol{q}_v^{\mathrm{T}} - 2q_0\boldsymbol{S}(\boldsymbol{q}_v). \tag{10}$$

Furthermore, the relative attitude dynamics can be obtained in frame $\mathcal{F}_{pb}$ as

$$\boldsymbol{J}_p\dot{\omega} + \boldsymbol{C}_r(\omega)\omega + \boldsymbol{n}_r(\omega) = \tau_d + \tau_a \tag{11}$$

where $\boldsymbol{\tau}_d$, $\boldsymbol{\tau}_a$ respectively denote the control torque and the disturbance torque; $\boldsymbol{C}_r(\omega), \boldsymbol{n}_r(\omega)$ yield

$$\begin{aligned} \boldsymbol{C}_r(\omega) &= \boldsymbol{J}_p\boldsymbol{S}(\boldsymbol{R}_{tb}^{pb}\omega_{i,tb}^{tb}) + \boldsymbol{S}(\boldsymbol{R}_{tb}^{pb}\omega_{i,tb}^{tb})\boldsymbol{J}_p - \\ &\quad \boldsymbol{S}(\boldsymbol{J}_p(\omega + \boldsymbol{R}_{tb}^{pb}\omega_{i,tb}^{tb})) \end{aligned} \tag{12}$$

$$\begin{aligned} \boldsymbol{n}_r(\omega) &= \boldsymbol{S}(\boldsymbol{R}_{tb}^{pb}\boldsymbol{\omega}_{i,tb}^{tb})\boldsymbol{J}_p\boldsymbol{R}_{tb}^{pb}\omega_{i,tb}^{tb} - \\ &\quad \boldsymbol{J}_p\boldsymbol{R}_{tb}^{pb}\boldsymbol{J}_t^{-1}\boldsymbol{S}(\omega_{i,tb}^{tb})\boldsymbol{J}_t\omega_{i,tb}^{tb} \end{aligned} \tag{13}$$

where $\boldsymbol{J}_p$ and $\boldsymbol{J}_t$ are inertia matrices of the pursuer and the target, respectively.

Define

$$\boldsymbol{x}_1 = \begin{bmatrix} \boldsymbol{p} \\ \boldsymbol{q} \end{bmatrix},\ \boldsymbol{x}_2 = \begin{bmatrix} \dot{\boldsymbol{p}} \\ \omega \end{bmatrix} \tag{14}$$

and combining (2), (6) and (11), the integrated model can be expressed as

$$\begin{cases} \dot{\boldsymbol{x}}_1 = \Lambda \boldsymbol{x}_2 \\ \boldsymbol{M}_p \dot{\boldsymbol{x}}_2 = \boldsymbol{F} + \boldsymbol{W} - \boldsymbol{C}\boldsymbol{x}_2 - \boldsymbol{D}\boldsymbol{x}_1 - \boldsymbol{n} \end{cases} \tag{15}$$

where

$$\Lambda = \begin{bmatrix} \boldsymbol{I} & 0 \\ 0 & \boldsymbol{T}(\boldsymbol{q}) \end{bmatrix}, \boldsymbol{M}_p = \begin{bmatrix} m_p \boldsymbol{I} & 0 \\ 0 & \boldsymbol{J}_p \end{bmatrix},$$
$$\boldsymbol{C} = \begin{bmatrix} \boldsymbol{C}_t(\dot{\gamma}) & 0 \\ 0 & \boldsymbol{C}_r(\omega) \end{bmatrix}, \boldsymbol{D} = \begin{bmatrix} \boldsymbol{D}_t(\dot{\gamma}, \ddot{\gamma}, r_p) & 0 \\ 0 & \boldsymbol{0} \end{bmatrix},$$
$$\boldsymbol{n} = \begin{bmatrix} \boldsymbol{n}_t(r_p, r_t) \\ \boldsymbol{n}_r(\omega) \end{bmatrix}, \boldsymbol{F} = \begin{bmatrix} \boldsymbol{F}_a \\ \tau_a \end{bmatrix}, \boldsymbol{W} = \begin{bmatrix} \boldsymbol{F}_d \\ \tau_d \end{bmatrix}.$$

As mentioned in Section 1, the major coupling between position and attitude dynamics results from the dependence of the thrust orientation for translation control on the spacecraft attitude and the thruster configuration. Therefore, for integrated control, the thruster layout should be considered. According to [12], suppose the pursuer spacecraft shows a cuboid shape with total six thrusters fixed as shown in Fig. 2. Considering each thruster generates a force f_i, $i = 1, 2, \cdots, 6$, and defining thrust vector as $\boldsymbol{f} = \begin{bmatrix} f_1 & f_2 & f_3 & f_4 & f_5 & f_6 \end{bmatrix}^{\mathrm{T}}$, the control input $\boldsymbol{F}$ in (15) can be thus expressed as

$$\boldsymbol{F} = \begin{bmatrix} \boldsymbol{F}_a \\ \boldsymbol{\tau}_a \end{bmatrix} = \begin{bmatrix} \boldsymbol{R}_{tb}^t \boldsymbol{R}_{pb}^{tb} & 0 \\ 0 & \boldsymbol{I} \end{bmatrix} \boldsymbol{A}_{\text{layout}} \boldsymbol{f} = \boldsymbol{A}\boldsymbol{f} \tag{16}$$

where $\boldsymbol{R}_{tb}^t$ denotes the transformation matrix from $\mathcal{F}_{tb}$ to $\mathcal{F}_t$, and the thruster installation matrix $\boldsymbol{A}_{\text{layout}}$ is given by

$$\boldsymbol{A}_{\text{layout}} = \begin{bmatrix} 0 & 0 & 1 & -1 & 0 & 0 \\ 0 & 0 & 0 & 0 & 1 & -1 \\ 1 & -1 & 0 & 0 & 0 & 0 \\ \frac{L_2}{2} & \frac{L_2}{2} & 0 & 0 & \frac{L_3}{2} & \frac{L_3}{2} \\ -\frac{L_1}{2} & -\frac{L_1}{2} & \frac{L_3}{2} & \frac{L_3}{2} & 0 & 0 \\ 0 & 0 & -\frac{L_2}{2} & -\frac{L_2}{2} & \frac{L_1}{2} & \frac{L_1}{2} \end{bmatrix}. \tag{17}$$

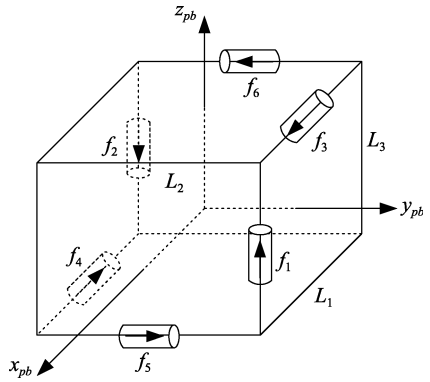

Fig. 2 Thrusters installation

Meanwhile, it is worthy noticing that, considering some of targets are non-cooperative, the inertia matrix of the target $\boldsymbol{J}_t$ may be not measurable, which incurs the term $\boldsymbol{J}_p \boldsymbol{R}_{tb}^{pb} \boldsymbol{J}_t^{-1} \boldsymbol{S}(\omega_{i,tb}^{tb}) \boldsymbol{J}_t \omega_{i,tb}^{tb}$ in (15) is unknown. To facilitate the parametrization of the term $\boldsymbol{n}$ in (15), with the definition of a linear operator $\mathcal{L} : \mathbf{R}^3 \to \mathbf{R}^{3\times 6}$ acting on an arbitrary vector $\boldsymbol{a} = \begin{bmatrix} a_1 & a_2 & a_3 \end{bmatrix}^{\mathrm{T}}$ such that

$$\mathcal{L}(\boldsymbol{a}) = \begin{bmatrix} a_1 & 0 & 0 & 0 & a_3 & a_2 \\ 0 & a_2 & 0 & a_3 & 0 & a_1 \\ 0 & 0 & a_3 & a_2 & a_1 & 0 \end{bmatrix}$$

the transformation[8]

$$\boldsymbol{J}_p \boldsymbol{R}_{tb}^{pb} \boldsymbol{J}_t^{-1} \boldsymbol{S}(\omega_{i,tb}^{tb}) \boldsymbol{J}_t \omega_{i,tb}^{tb} = \boldsymbol{U}\theta \tag{18}$$

where

$$\theta = \boldsymbol{U}_1 \boldsymbol{\theta}_t \in \mathbf{R}^{324}, \quad \boldsymbol{U} = \boldsymbol{U}_4 \boldsymbol{U}_5 \in \mathbf{R}^{3\times 324},$$

$$\theta_t = \begin{bmatrix} \boldsymbol{J}_{t11} & \boldsymbol{J}_{t22} & \boldsymbol{J}_{t33} & \boldsymbol{J}_{t23} & \boldsymbol{J}_{t13} & \boldsymbol{J}_{t12} \end{bmatrix}^{\mathrm{T}} \in \mathbf{R}^6,$$
$$\boldsymbol{U}_1 = \begin{bmatrix} \Delta_1^{\mathrm{T}} \\ \vdots \\ \Delta_{18}^{\mathrm{T}} \end{bmatrix} \in \mathbf{R}^{324\times 6},$$
$$\Delta_i = \begin{bmatrix} \delta_i & \cdots & O_{1\times 3} \\ \vdots & \ddots & \vdots \\ O_{1\times 3} & \cdots & \delta_i \end{bmatrix} \in \mathbf{R}^{6\times 18},\ i = 1, 2, \cdots, 18,$$
$$\delta_i = \mathrm{row}_i(\boldsymbol{U}_2) \in \mathbf{R}^{1\times 3},\ \boldsymbol{U}_2 = \boldsymbol{U}_3 \boldsymbol{J}_t^{-1} \in \mathbf{R}^{18\times 3},$$
$$\boldsymbol{U}_3 = \begin{bmatrix} \theta_p & O_{6\times 1} & O_{6\times 1} \\ O_{6\times 1} & \theta_p & O_{6\times 1} \\ O_{6\times 1} & O_{6\times 1} & \theta_p \end{bmatrix} \in \mathbf{R}^{18\times 3},$$
$$\theta_p = \begin{bmatrix} \boldsymbol{J}_{p11} & \boldsymbol{J}_{p22} & \boldsymbol{J}_{p33} & \boldsymbol{J}_{p23} & \boldsymbol{J}_{p13} & \boldsymbol{J}_{p12} \end{bmatrix}^{\mathrm{T}} \in \mathbf{R}^6,$$
$$\boldsymbol{U}_4 = \begin{bmatrix} \mathcal{L}(R_1) & \mathcal{L}(R_2) & \mathcal{L}(R_3) \end{bmatrix} \in \mathbf{R}^{3\times 18},$$
$$R_k = \mathrm{col}_k(\boldsymbol{R}_{tb}^{pb}) \in \mathbf{R}^3,\ k = 1, 2, 3,$$
$$\boldsymbol{U}_5 = \begin{bmatrix} \phi & \cdots & O_{1\times 18} \\ \vdots & \ddots & \vdots \\ O_{1\times 18} & \cdots & \phi \end{bmatrix} \in \mathbf{R}^{18\times 324},$$
$$\phi = \begin{bmatrix} \phi_1^{\mathrm{T}} & \phi_2^{\mathrm{T}} & \phi_3^{\mathrm{T}} & \phi_4^{\mathrm{T}} & \phi_5^{\mathrm{T}} & \phi_6^{\mathrm{T}} \end{bmatrix} \in \mathbf{R}^{1\times 18},$$
$$\phi_j = \mathrm{col}_j \left(\boldsymbol{S}(\omega_{i,tb}^{tb}) \mathcal{L}(\omega_{i,tb}^{tb}) \right) \in \mathbf{R}^3,\ j = 1, 2, \cdots, 6$$

transforms the nonlinear term $\boldsymbol{n}$ into

$$\boldsymbol{n} = \boldsymbol{n}_0 + \boldsymbol{N}\theta \tag{19}$$

where

$$\boldsymbol{n}_0 = \begin{bmatrix} \boldsymbol{n}_t(r_t, r_p) \\ \boldsymbol{S}(\boldsymbol{R}_{tb}^{pb} \omega_{i,tb}^{tb}) \boldsymbol{J}_p \boldsymbol{R}_{tb}^{pb} \omega_{i,tb}^{tb} \end{bmatrix}, \boldsymbol{N} = \begin{bmatrix} \boldsymbol{0} \\ \boldsymbol{U} \end{bmatrix}.$$

Besides, for the bounded disturbance $\boldsymbol{W}$, including gravitational variations, atmospheric drag, solar radiation, and

third-body effects[21,25], satisfying

$$||\boldsymbol{W}|| \leqslant d_w \tag{20}$$

where the bound d_w is a known constant.

Since we aim to make the pursuer have no relative motion with respect to the target, the desired relative position and attitude quaternion should be, respectively,

$$\boldsymbol{p}_c = \boldsymbol{0},\ \boldsymbol{q}_c = \begin{bmatrix} 1 & 0 & 0 & 0 \end{bmatrix}^{\mathrm{T}}.$$

Then, the relative position error and attitude error can be respectively obtained as

$$\boldsymbol{e}_p = \boldsymbol{p} - \boldsymbol{p}_c = \boldsymbol{p}, \quad \tilde{\boldsymbol{q}} = \boldsymbol{q}_c^{-1} \circ \boldsymbol{q} = \boldsymbol{q}.$$

It is worth mentioning that, the relative attitude error $\tilde{\boldsymbol{q}}^{\mathrm{T}} = \boldsymbol{q}^{\mathrm{T}} = \begin{bmatrix} q_0 & \boldsymbol{q}_v^{\mathrm{T}} \end{bmatrix}$ has two equilibrium points, i.e., $\begin{bmatrix} \pm 1 & 0 & 0 & 0 \end{bmatrix}^{\mathrm{T}}$, representing the same physical orientation. To facilitate the following controller design, the equilibrium point of $\tilde{\boldsymbol{q}}$ should be determined first. According to [13], to minimize the path length, the selection of equilibrium point can be determined by the given initial condition. Specifically, choose $\begin{bmatrix} 1 & 0 & 0 & 0 \end{bmatrix}^{\mathrm{T}}$ as equilibrium point when $q_0(0) \geqslant 0$, while $\begin{bmatrix} -1 & 0 & 0 & 0 \end{bmatrix}^{\mathrm{T}}$ is chosen for $q_0(0) < 0$; meanwhile, it is further assumed that the scalar part q_0 does not change sign, i.e.,

$$\mathrm{sgn}(q_0(0)) = \mathrm{sgn}(q_0(t)),\ \forall t > 0 \tag{21}$$

which leads to that

$$1 - q_0 \leqslant 1 - q_0^2 = \boldsymbol{q}_v^{\mathrm{T}} \boldsymbol{q}_v. \tag{22}$$

Without loss of generality, this paper only considers the case $q_0(0) \geqslant 0$, equivalently, $\begin{bmatrix} 1 & 0 & 0 & 0 \end{bmatrix}^{\mathrm{T}}$ is chosen as the equilibrium of $\tilde{\boldsymbol{q}}$ and $q_0(t) \geqslant 0$.

Let

$$\tilde{\boldsymbol{x}}_1 = \begin{bmatrix} \boldsymbol{e}_p \\ \boldsymbol{e}_q \end{bmatrix} \in \mathbf{R}^7, \quad \boldsymbol{e}_q = \begin{bmatrix} q_0 - 1 \\ \boldsymbol{q}_v \end{bmatrix}. \tag{23}$$

Meanwhile, define

$$\overline{\boldsymbol{x}}_1 = \begin{bmatrix} \boldsymbol{p}^{\mathrm{T}} & \boldsymbol{q}_v^{\mathrm{T}} \end{bmatrix}^{\mathrm{T}} \in \mathbf{R}^6 \tag{24}$$

and according to (22), one has

$$\tilde{\boldsymbol{x}}_1^{\mathrm{T}} \tilde{\boldsymbol{x}}_1 \leqslant \overline{\boldsymbol{x}}_1^{\mathrm{T}} \Gamma^{-1} \overline{\boldsymbol{x}}_1 \tag{25}$$

and another useful property

$$\Lambda^{\mathrm{T}} \boldsymbol{x}_1 = \Gamma \overline{\boldsymbol{x}}_1 \tag{26}$$

where $\Gamma = \mathrm{diag}\{\ \boldsymbol{I}_{3\times 3} \quad \frac{1}{2}\boldsymbol{I}_{3\times 3}\ \}$. Then, combining (16), (23) and (24), the coupled dynamics (15) can be rewritten as

$$\begin{cases} \dot{\tilde{\boldsymbol{x}}}_1 = \Lambda \boldsymbol{x}_2 \\ \boldsymbol{M}_p \dot{\boldsymbol{x}}_2 = \boldsymbol{A}\boldsymbol{f} + \boldsymbol{W} - \boldsymbol{C}\boldsymbol{x}_2 - \boldsymbol{D}\boldsymbol{x}_1 - \boldsymbol{n}_0 - \boldsymbol{N}\theta. \end{cases} \tag{27}$$

Recalling that we aim to make the pursuer approach the target with simultaneous attitude maneuvering, the problem can be formulated as follows.

Problem 1. For the coupled relative translation and attitude error dynamics (27), design a control law $\boldsymbol{f}$ such that the states $\tilde{\boldsymbol{x}}_1, \boldsymbol{x}_2$ converge to zero as closely as possible in spite of the bounded disturbance $\boldsymbol{W}$ and the unknown term θ in (18).

Remark 1. In view of the thruster configuration, it should be pointed out that the configuration shown in Fig. 2 is not unique. However, any thruster layout should ensure $\boldsymbol{A}_{\mathrm{layout}}$ is invertible. To this end, for the 6-DOF dynamics in (15), it is necessary to assemble at least six thrusters. If possible, more thrusters may be expected; as a result, the column of $\boldsymbol{A}_{\mathrm{layout}}$ may be larger than 6, yet it is noticeable that the following rank condition should be satisfied

$$\mathrm{rank}(\boldsymbol{A}_{\mathrm{layout}}) \geqslant 6. \tag{28}$$

Thus the inverse of $\boldsymbol{A}_{\mathrm{layout}}$ can be obtained using pseudoinverse $\boldsymbol{A}_{\mathrm{layout}}^{+}$:

$$\boldsymbol{A}_{\mathrm{layout}}^{+} = (\boldsymbol{A}_{\mathrm{layout}}^{\mathrm{T}} \boldsymbol{A}_{\mathrm{layout}})^{-1} \boldsymbol{A}_{\mathrm{layout}}^{\mathrm{T}}. \tag{29}$$

3 Controller design

To deal with Problem 1, in this section, motivated by singular perturbation theory, an adaptive backstepping controller with a command filter is proposed; meanwhile, the ultimate boundedness of relative position and attitude signals is guaranteed by Lyapunov theorem.

In view of the error kinematics in (27), i.e., $\dot{\tilde{\boldsymbol{x}}}_1 = \Lambda \boldsymbol{x}_2$, using the standard backstepping method[23], the desired virtual control can be easily obtained as

$$\boldsymbol{x}_{2c}^0 = -\boldsymbol{K}_1 \Lambda^{\mathrm{T}} \tilde{\boldsymbol{x}}_1 \tag{30}$$

where $\boldsymbol{K}_1$ is a positive definite matrix to be designed; then, it can be easily derived that, the first order derivative of desired virtual control $\dot{\boldsymbol{x}}_{2c}^0$ will be contained in the final control $\boldsymbol{f}$, which is not anticipated. In order to eliminate this "explosion of terms" and make the controller simple, the following second order filter, namely command filter[20],

$$\begin{cases} \dot{\boldsymbol{z}}_1 = \omega_n \boldsymbol{z}_2 \\ \dot{\boldsymbol{z}}_2 = -2\zeta\omega_n \boldsymbol{z}_2 + \omega_n(\boldsymbol{x}_{2c}^0 - \boldsymbol{x}_{2c}) \end{cases} \tag{31}$$

is used to estimate terms $\boldsymbol{x}_{2c}^0, \dot{\boldsymbol{x}}_{2c}^0$ by using $\boldsymbol{x}_{2c}, \dot{\boldsymbol{x}}_{2c}$ given by

$$\begin{cases} \boldsymbol{x}_{2c} = \boldsymbol{z}_1 \\ \dot{\boldsymbol{x}}_{2c} = \omega_n \boldsymbol{z}_2 \end{cases} \tag{32}$$

where $\zeta, \omega_n \in \mathbf{R}$ are filter parameters. Meanwhile, define

$$\tilde{\boldsymbol{x}}_2 = \boldsymbol{x}_2 - \boldsymbol{x}_{2c}. \tag{33}$$

Next, let $\varepsilon = 1/\omega_n$, then the command filter (31) can be rewritten as

$$\begin{cases} \varepsilon \dot{\boldsymbol{z}}_1 = \boldsymbol{z}_2 \\ \varepsilon \dot{\boldsymbol{z}}_2 = -2\zeta \boldsymbol{z}_2 + (\boldsymbol{x}_{2c}^0 - \boldsymbol{z}_1). \end{cases} \tag{34}$$

According to singular perturbation theory[23], at $\varepsilon = 0$, the unique roots of equations (34) can be obtained as

$$\boldsymbol{z}_1|_{\varepsilon=0} = \boldsymbol{x}_{2c}^0,\ \boldsymbol{z}_2|_{\varepsilon=0} = 0. \tag{35}$$

Moreover, the following change of variables is used to make the equilibrium point of the filter (34) as zero. Let

$$\boldsymbol{y}=\left[\begin{array}{c}\boldsymbol{y}_1\\ \boldsymbol{y}_2\end{array}\right]=\left[\begin{array}{c}\boldsymbol{z}_1-\boldsymbol{x}_{2c}^0\\ \boldsymbol{z}_2\end{array}\right] \tag{36}$$

so (34) is equivalent to

$$\left\{\begin{array}{l}\varepsilon\dot{\boldsymbol{y}}_1=\boldsymbol{y}_2-\varepsilon\dot{\boldsymbol{x}}_{2c}^0\\ \varepsilon\dot{\boldsymbol{y}}_2=-2\zeta\boldsymbol{y}_2-\boldsymbol{y}_1.\end{array}\right. \tag{37}$$

In order to simplify (37), noticing that

$$\boldsymbol{x}_2=\tilde{\boldsymbol{x}}_2+\boldsymbol{z}_1=\tilde{\boldsymbol{x}}_2+\boldsymbol{y}_1+\boldsymbol{x}_{2c}^0 \tag{38}$$

and utilizing the property (26), one can thus obtain

$$\begin{aligned}\dot{\boldsymbol{x}}_{2c}^0=&-\boldsymbol{K}_1\Gamma\dot{\tilde{\boldsymbol{x}}}_1=\\ &-\boldsymbol{K}_1\Gamma\Lambda_0\boldsymbol{x}_2=\\ &\boldsymbol{K}_1\Gamma\Lambda_0\boldsymbol{K}_1\Lambda^{\mathrm{T}}\tilde{\boldsymbol{x}}_1-\boldsymbol{K}_1\Gamma\Lambda_0\tilde{\boldsymbol{x}}_2-\boldsymbol{K}_1\Gamma\Lambda_0\boldsymbol{y}_1\end{aligned} \tag{39}$$

where

$$\Lambda_0=\left[\begin{array}{cc}\boldsymbol{I}&0\\ 0&\frac{1}{2}\left(q_0\boldsymbol{I}+\boldsymbol{S}(\boldsymbol{q}_v)\right)\end{array}\right]\leqslant\left[\begin{array}{cc}\boldsymbol{I}&0\\ 0&\frac{1}{2}\boldsymbol{I}\end{array}\right]. \tag{40}$$

Then the command filter (37) can be simplified as

$$\varepsilon\dot{\boldsymbol{y}}=\boldsymbol{A}_0\boldsymbol{y}-\varepsilon\boldsymbol{h} \tag{41}$$

where

$$\begin{aligned}\boldsymbol{A}_0=&\left[\begin{array}{cc}0&\boldsymbol{I}\\ -\boldsymbol{I}&-2\zeta\boldsymbol{I}\end{array}\right],\\ \boldsymbol{h}=&\left[\begin{array}{c}\boldsymbol{K}_1\Gamma\Lambda_0\boldsymbol{K}_1\Lambda^{\mathrm{T}}\tilde{\boldsymbol{x}}_1-\boldsymbol{K}_1\Gamma\Lambda_0\tilde{\boldsymbol{x}}_2-\boldsymbol{K}_1\Gamma\Lambda_0\boldsymbol{y}_1\\ \boldsymbol{0}\end{array}\right].\end{aligned}$$

Therefore, (27) and (41) constitute a full singularly perturbed system. To control this system, an integrated control strategy is put forward in the following theorem.

Theorem 1. For the system (27) in conjunction with the command filter (31), given scalars k, k_q, k_h, k_θ, α, β, ζ, $\omega_n>0$, and matrices

$$\boldsymbol{K}_1=\left[\begin{array}{cc}k\boldsymbol{I}&0\\ 0&8k\boldsymbol{I}\end{array}\right],\ \boldsymbol{K}_2=\left(k+\frac{1}{2}\right)\boldsymbol{I}_{6\times6} \tag{42}$$

$$\boldsymbol{P}_0=\left[\begin{array}{cc}(\zeta+\frac{1}{2\zeta})\boldsymbol{I}&0\\ \frac{1}{2}\boldsymbol{I}&0\end{array}\right] \tag{43}$$

$$\boldsymbol{G}=\left[\begin{array}{cc}(\zeta+\frac{1}{2\zeta})\boldsymbol{I}&\frac{1}{2}\boldsymbol{I}\end{array}\right] \tag{44}$$

if

$$\omega_n\beta k_q-2kk_q\beta||\boldsymbol{P}_0||-\frac{1}{\alpha k}\left(\frac{\alpha}{2}+\sqrt{1+k^2}kk_q\beta\left\|\boldsymbol{G}\right\|\right)^2>0 \tag{45}$$

then, the following adaptive control law

$$\begin{aligned}\boldsymbol{f}=&\boldsymbol{A}^{-1}(\boldsymbol{C}\boldsymbol{x}_{2c}+\boldsymbol{D}\boldsymbol{x}_1+\boldsymbol{n}_0+\boldsymbol{N}\hat{\theta}+\boldsymbol{M}_p\dot{\boldsymbol{x}}_{2c}-\\ &\Lambda^{\mathrm{T}}\tilde{\boldsymbol{x}}_1-\boldsymbol{K}_2\tilde{\boldsymbol{x}}_2)\end{aligned} \tag{46}$$

$$\dot{\hat{\theta}}=-\alpha k_h\boldsymbol{N}^{\mathrm{T}}\tilde{\boldsymbol{x}}_2-k_\theta\hat{\theta} \tag{47}$$

ensures that the system signals $\tilde{\boldsymbol{x}}_1,\boldsymbol{x}_2$ are ultimately bounded; moreover, the corresponding bounds can be made arbitrarily small by adjusting parameters appropriately.

Proof. In view of the filter (41), substituting the control law into the system (27) obtains the closed-loop system

$$\left\{\begin{array}{l}\dot{\tilde{\boldsymbol{x}}}_1=-\Lambda\boldsymbol{K}_1\Lambda^{\mathrm{T}}\tilde{\boldsymbol{x}}_1+\Lambda\tilde{\boldsymbol{x}}_2+\Lambda\boldsymbol{y}_1\\ \boldsymbol{M}_p\dot{\tilde{\boldsymbol{x}}}_2=-\Lambda^{\mathrm{T}}\tilde{\boldsymbol{x}}_1-\boldsymbol{K}_2\tilde{\boldsymbol{x}}_2+\boldsymbol{W}-C\tilde{\boldsymbol{x}}_2+\boldsymbol{N}\tilde{\theta}\\ \varepsilon\dot{\boldsymbol{y}}=\boldsymbol{A}_0\boldsymbol{y}-\varepsilon\boldsymbol{h}\\ \dot{\hat{\theta}}=-\alpha k_h\boldsymbol{N}^{\mathrm{T}}\tilde{\boldsymbol{x}}_2-k_\theta\hat{\theta}.\end{array}\right. \tag{48}$$

Then, by defining the estimate error as $\tilde{\theta}=\hat{\theta}-\theta$ and letting

$$\xi=\left[\begin{array}{cccc}\tilde{\boldsymbol{x}}_1^{\mathrm{T}}&\tilde{\boldsymbol{x}}_2^{\mathrm{T}}&\boldsymbol{y}^{\mathrm{T}}&\tilde{\theta}^{\mathrm{T}}\end{array}\right]^{\mathrm{T}}\in\mathbf{R}^{343} \tag{49}$$

a composite Lyapunov function V is constructed as

$$V(\xi)=\frac{\alpha}{2}\tilde{\boldsymbol{x}}_1^{\mathrm{T}}\tilde{\boldsymbol{x}}_1+\frac{\alpha}{2}\tilde{\boldsymbol{x}}_2^{\mathrm{T}}\boldsymbol{M}_p\tilde{\boldsymbol{x}}_2+\beta\boldsymbol{y}^{\mathrm{T}}\boldsymbol{P}\boldsymbol{y}+\frac{1}{2k_h}\tilde{\theta}^{\mathrm{T}}\tilde{\theta} \tag{50}$$

where the matrix $\boldsymbol{P}>0$ is selected to satisfy the following Lyapunov equation

$$\boldsymbol{A}_0^{\mathrm{T}}\boldsymbol{P}+\boldsymbol{P}\boldsymbol{A}_0=-\boldsymbol{Q} \tag{51}$$

in which $\boldsymbol{Q}\in\mathbf{R}^{6\times6}$ is a positive definite matrix chosen as $\boldsymbol{Q}=k_q\boldsymbol{I}$. Moreover, let the solution matrix $\boldsymbol{P}$ to the Lyapunov equation (51) be

$$\boldsymbol{P}=\left[\begin{array}{cc}\boldsymbol{P}_1&\boldsymbol{P}_2\end{array}\right]=\left[\begin{array}{cc}\boldsymbol{P}_{11}&\boldsymbol{P}_{12}\\ \boldsymbol{P}_{12}&\boldsymbol{P}_{22}\end{array}\right] \tag{52}$$

which results in

$$\boldsymbol{P}_{11}=(k_q\zeta+\frac{k_q}{2\zeta})\boldsymbol{I},\ \boldsymbol{P}_{12}=\frac{k_q}{2}\boldsymbol{I},\ \boldsymbol{P}_{22}=\frac{k_q}{2\zeta}\boldsymbol{I}. \tag{53}$$

Taking the derivative of V with respect to time gives

$$\begin{aligned}\dot{V}=&\alpha\tilde{\boldsymbol{x}}_1^{\mathrm{T}}\dot{\tilde{\boldsymbol{x}}}_1+\alpha\tilde{\boldsymbol{x}}_2^{\mathrm{T}}\boldsymbol{M}_p\dot{\tilde{\boldsymbol{x}}}_2+\beta\dot{\boldsymbol{y}}^{\mathrm{T}}\boldsymbol{P}\boldsymbol{y}+\beta\boldsymbol{y}^{\mathrm{T}}\boldsymbol{P}\dot{\boldsymbol{y}}+\frac{1}{k_h}\tilde{\theta}^{\mathrm{T}}\dot{\hat{\theta}}=\\ &\alpha\boldsymbol{x}_1^{\mathrm{T}}(-\Lambda\boldsymbol{K}_1\Lambda^{\mathrm{T}}\tilde{\boldsymbol{x}}_1+\Lambda\tilde{\boldsymbol{x}}_2+\Lambda\boldsymbol{y}_1)-\alpha\tilde{\boldsymbol{x}}_2^{\mathrm{T}}\boldsymbol{C}\tilde{\boldsymbol{x}}_2+\\ &\alpha\tilde{\boldsymbol{x}}_2^{\mathrm{T}}(-\Lambda^{\mathrm{T}}\tilde{\boldsymbol{x}}_1-\boldsymbol{K}_2\tilde{\boldsymbol{x}}_2+\boldsymbol{W}+\boldsymbol{N}\widetilde{\theta})+\\ &\frac{\beta}{\varepsilon}\boldsymbol{y}^{\mathrm{T}}(\boldsymbol{A}_0^{\mathrm{T}}\boldsymbol{P}+\boldsymbol{P}\boldsymbol{A}_0)\boldsymbol{y}-2\beta\boldsymbol{y}^{\mathrm{T}}\boldsymbol{P}\boldsymbol{h}+\frac{1}{k_h}\tilde{\theta}^{\mathrm{T}}\dot{\hat{\theta}}\leqslant\\ &-\alpha\tilde{\boldsymbol{x}}_1^{\mathrm{T}}\Lambda\boldsymbol{K}_1\Lambda^{\mathrm{T}}\tilde{\boldsymbol{x}}_1-\alpha\tilde{\boldsymbol{x}}_2^{\mathrm{T}}\boldsymbol{K}_2\tilde{\boldsymbol{x}}_2+\alpha\tilde{\boldsymbol{x}}_2^{\mathrm{T}}\boldsymbol{W}+\\ &\alpha\tilde{\boldsymbol{x}}_1^{\mathrm{T}}\Lambda\boldsymbol{y}_1-\frac{\beta}{\varepsilon}\boldsymbol{y}^{\mathrm{T}}\boldsymbol{Q}\boldsymbol{y}-2\beta\boldsymbol{y}^{\mathrm{T}}\boldsymbol{P}\boldsymbol{h}+\frac{1}{k_h}\tilde{\theta}^{\mathrm{T}}(\dot{\hat{\theta}}+\alpha k_h\boldsymbol{N}^{\mathrm{T}}\tilde{\boldsymbol{x}}_2).\end{aligned} \tag{54}$$

By using (52) and (53), one has

$$\boldsymbol{P}\boldsymbol{h}=\boldsymbol{P}_1(\boldsymbol{K}_1\Gamma\Lambda_0\boldsymbol{K}_1\Lambda^{\mathrm{T}}\tilde{\boldsymbol{x}}_1-\boldsymbol{K}_1\Gamma\Lambda_0\tilde{\boldsymbol{x}}_2-\boldsymbol{K}_1\Gamma\Lambda_0\boldsymbol{y}_1) \tag{55}$$

and thus

$$\begin{aligned}\dot{V}\leqslant&-\alpha\overline{\boldsymbol{x}}_1^{\mathrm{T}}\Gamma^{\mathrm{T}}\boldsymbol{K}_1\Gamma\overline{\boldsymbol{x}}_1-\alpha\tilde{\boldsymbol{x}}_2^{\mathrm{T}}\boldsymbol{K}_2\tilde{\boldsymbol{x}}_2-\frac{\beta}{\varepsilon}\boldsymbol{y}^{\mathrm{T}}\boldsymbol{Q}\boldsymbol{y}-\frac{k_\theta}{k_h}\tilde{\theta}^{\mathrm{T}}\tilde{\theta}+\\ &\alpha\tilde{\boldsymbol{x}}_1^{\mathrm{T}}\Lambda\boldsymbol{y}_1-\frac{k_\theta}{k_h}\tilde{\theta}^{\mathrm{T}}\theta+\alpha\tilde{\boldsymbol{x}}_2^{\mathrm{T}}\boldsymbol{W}-\\ &2\beta\boldsymbol{y}^{\mathrm{T}}\boldsymbol{P}_1\boldsymbol{K}_1(\Gamma\Lambda_0\boldsymbol{K}_1\Lambda^{\mathrm{T}}\tilde{\boldsymbol{x}}_1-\Gamma\Lambda_0\tilde{\boldsymbol{x}}_2-\Gamma\Lambda_0\boldsymbol{y}_1).\end{aligned} \tag{56}$$

Noting that

$$\tilde{\theta}^{\mathrm{T}}\theta\leqslant\frac{1}{2}\tilde{\theta}^{\mathrm{T}}\tilde{\theta}+\frac{1}{2}\theta^{\mathrm{T}}\theta,\quad\tilde{\boldsymbol{x}}_2^{\mathrm{T}}\boldsymbol{W}\leqslant\frac{1}{2}\tilde{\boldsymbol{x}}_2^{\mathrm{T}}\tilde{\boldsymbol{x}}_2+\frac{1}{2}d_w^2 \tag{57}$$

and utilizing (25) and (44), transform (56) into

$$\dot{V} \leqslant \begin{bmatrix} \tilde{\boldsymbol{x}}_1 \\ \tilde{\boldsymbol{x}}_2 \\ \boldsymbol{y} \\ \tilde{\theta} \end{bmatrix}^{\mathrm{T}} \begin{bmatrix} \boldsymbol{S} & O \\ O & -\frac{k_\theta}{2k_h} \end{bmatrix} \begin{bmatrix} \tilde{\boldsymbol{x}}_1 \\ \tilde{\boldsymbol{x}}_2 \\ \boldsymbol{y} \\ \tilde{\theta} \end{bmatrix} + \frac{k_\theta}{2k_h}\theta^{\mathrm{T}}\theta + \frac{\alpha}{2}d_w^2 \leqslant \xi^{\mathrm{T}}\boldsymbol{H}\xi + \eta \leqslant \kappa V + \eta \tag{58}$$

where

$$\kappa = \frac{\lambda_{\max}(\boldsymbol{H})}{\varsigma_2},$$

$$\varsigma_2 = \max\left\{\frac{\alpha}{2},\ \frac{\alpha}{2}\lambda_{\max}(\boldsymbol{M}_p),\ \beta\lambda_{\max}(\boldsymbol{P}),\ \frac{1}{2k_h}\right\},$$

$$\boldsymbol{S} = \begin{bmatrix} \boldsymbol{S}_{11} & \boldsymbol{S}_{12} \\ \boldsymbol{S}_{12}^{\mathrm{T}} & \boldsymbol{S}_{22} \end{bmatrix}, \eta = \frac{k_\theta}{2k_h}\max\{\theta^{\mathrm{T}}\theta\} + \frac{\alpha}{2}d_w^2,$$

$$\boldsymbol{S}_{11} = \begin{bmatrix} -\alpha k\boldsymbol{I} & 0 \\ 0 & -\alpha\left(\boldsymbol{K}_2 - \frac{1}{2}\boldsymbol{I}\right) \end{bmatrix},$$

$$\boldsymbol{S}_{12} = \begin{bmatrix} \frac{\alpha}{2}\begin{bmatrix} \Lambda & 0 \end{bmatrix} - \beta\Lambda\boldsymbol{K}_1\Lambda_0^{\mathrm{T}}\Gamma\boldsymbol{K}_1\boldsymbol{P}_1^{\mathrm{T}} \\ \beta\Lambda_0^{\mathrm{T}}\Gamma\boldsymbol{K}_1\boldsymbol{P}_1^{\mathrm{T}} \end{bmatrix},$$

$$\boldsymbol{S}_{22} = -\frac{\beta}{\varepsilon}\boldsymbol{Q} + 2\beta\begin{bmatrix} \boldsymbol{P}_1\boldsymbol{K}_1\Gamma\Lambda_0 & 0 \end{bmatrix}.$$

Then, with the gain matrices $\boldsymbol{K}_1$ and $\boldsymbol{K}_2$ in (44), one has

$$\boldsymbol{S}_{11} = -\alpha k\boldsymbol{I},$$

$$\boldsymbol{S}_{22} - \boldsymbol{S}_{12}\boldsymbol{S}_{11}^{-1}\boldsymbol{S}_{12}^{\mathrm{T}} = -\frac{\beta}{\varepsilon}\boldsymbol{Q} + 2\beta\begin{bmatrix} \boldsymbol{P}_1\boldsymbol{K}_1\Gamma\Lambda_0 & 0 \end{bmatrix} + \frac{1}{\alpha k}\boldsymbol{S}_{12}\boldsymbol{S}_{12}^{\mathrm{T}}$$

and

$$\boldsymbol{S}_{12} = \frac{\alpha}{2}\begin{bmatrix} \Lambda & 0 \\ 0 & 0 \end{bmatrix} - \beta\begin{bmatrix} \Lambda\boldsymbol{K}_1 \\ \boldsymbol{I} \end{bmatrix}\Lambda_0^{\mathrm{T}}\Gamma\boldsymbol{K}_1\boldsymbol{P}_1^{\mathrm{T}} = \frac{\alpha}{2}\begin{bmatrix} \Lambda & 0 \\ 0 & 0 \end{bmatrix} - \beta\begin{bmatrix} \Lambda\boldsymbol{K}_1 \\ \boldsymbol{I} \end{bmatrix}\Lambda_0^{\mathrm{T}}\Gamma\boldsymbol{K}_1\begin{bmatrix} (k_q\zeta + \frac{k_q}{2\zeta})\boldsymbol{I} & \frac{k_q}{2}\boldsymbol{I} \end{bmatrix} = \frac{\alpha}{2}\begin{bmatrix} \Lambda & 0 \\ 0 & 0 \end{bmatrix} - kk_q\beta\begin{bmatrix} \Lambda\boldsymbol{K}_1 \\ \boldsymbol{I} \end{bmatrix}\Lambda_0^{\mathrm{T}}\boldsymbol{G}.$$

According to Shur complement lemma, $\boldsymbol{S} < \boldsymbol{0}$ is equivalent to

$$\boldsymbol{S}_{11} < 0 \tag{59}$$

$$\boldsymbol{S}_{22} - \boldsymbol{S}_{12}\boldsymbol{S}_{11}^{-1}\boldsymbol{S}_{12}^{\mathrm{T}} < 0. \tag{60}$$

Hence, noticing that

$$\|[\ \boldsymbol{P}_1\boldsymbol{K}_1\Gamma\Lambda_0 \quad 0\ ]\| < k\|[\ \boldsymbol{P}_1 \quad 0\ ]\| = kk_q\|\boldsymbol{P}_0\|$$

and

$$\|\boldsymbol{S}_{12}\| \leqslant \frac{\alpha}{2} + \sqrt{1+k^2}kk_q\beta\|\boldsymbol{G}\|$$

if condition (45) holds, then $\boldsymbol{S} < \boldsymbol{0}$. Furthermore, by the comparison principle[23], it is easy to derive from (58) that

$$V(t) \leqslant V(0)\mathrm{e}^{\kappa t} - \frac{\eta}{\kappa}\left(1 - \mathrm{e}^{\kappa t}\right). \tag{61}$$

Therefore, $\tilde{\boldsymbol{x}}_1, \tilde{\boldsymbol{x}}_2, \boldsymbol{y}, \tilde{\theta}$ are ultimately bounded and so is the state $\boldsymbol{x}_2$ due to (38). In addition, the bound $-\eta/\kappa$ can be made arbitrarily small by choosing appropriate κ, which concludes that the ultimate bound of the states $\tilde{\boldsymbol{x}}_1, \tilde{\boldsymbol{x}}_2, \boldsymbol{x}_2, \boldsymbol{y}, \tilde{\theta}$ can be made arbitrarily small. □

Remark 2. Compared with the standard backstepping, the designed control law (46) no longer requires the analytic computation of virtual controls. Meanwhile, it should be noted that, even if the exact analytical expression of the virtual control can be derived, it is lacking of robustness since the designed model is essentially an approximation of the real plant[20]. Instead, the linear command filter (31) is not only easy to realize, but also capable of overcoming the above defect.

Remark 3. It can be seen from (61) that the ultimate boundedness of the system states is achieved by the proposed controller, which also can be considered as practical stability[26]. Moreover, although the ultimate boundedness of system states is given, yet the exact bound is hard to be computed out owing to the existence of the unknown term $\max(\theta^{\mathrm{T}}\theta)$ in η. Hence, if the bound of unknown parameter vector θ can be estimated in advance, then the bound of $\tilde{\boldsymbol{x}}_1$ can be exactly computed out from (61), i.e.,

$$\|\tilde{\boldsymbol{x}}_1\| \leqslant \sqrt{\frac{V}{\varsigma_1}} \leqslant \sqrt{-\frac{\eta}{\kappa\varsigma_1}} \tag{62}$$

where $\varsigma_1 = \min\left\{\frac{\alpha}{2},\ \frac{\alpha}{2}\lambda_{\min}(\boldsymbol{M}_p),\ \beta\lambda_{\min}(\boldsymbol{P}),\ \frac{1}{2k_h}\right\}$; furthermore, the bound of the state $\boldsymbol{x}_2$ can be obtained by using (38) and (50)

$$\|\boldsymbol{x}_2\| \leqslant \left\|\tilde{\boldsymbol{x}}_2 + \boldsymbol{y}_1 - \boldsymbol{K}_1\Lambda^{\mathrm{T}}\tilde{\boldsymbol{x}}_1\right\| \leqslant 4k\|\boldsymbol{\xi}\| \leqslant 4k\sqrt{-\frac{\eta}{\kappa\varsigma_1}}. \tag{63}$$

4 Numerical simulation

In this section, a simulation scenario is considered to demonstrate the effect of the proposed control strategy. The scenario aims to make a pursuer approach an in-orbit spacecraft in need of repair or refueling, and meanwhile makes the attitude of the pursuer perform nearly stationary relative to the earth. This proximity rendezvous and docking operation is extensively reflected in most of space missions, such as refueling a nadir-pointing communication satellite on a geosynchronous orbit (GEO), capturing a spatial debris or constructing the international space station. Fig. 3 gives the whole structure of the closed loop system. Assume that the target space objective is flying in a low round orbit with the altitude 250 km. Orbit inclination is considered to be 30°, while the argument of perigee and right ascension of ascending node is 0°. Then, the orbit angular velocity of the target is obtained as $\omega_t = \sqrt{\mu/r_t^3}$. Suppose that the target is nadir-pointing, so the transformation matrix $\boldsymbol{R}_{tb}^t$ from the target body frame $\mathcal{F}_{tb}$ to the LVLH frame $\mathcal{F}_t$ poses a constant matrix. Without loss of generality, consider that $\boldsymbol{R}_{tb}^t = \boldsymbol{I}$.

Suppose the size of the pursuer spacecraft is $L_1 = L_2 = L_3 = 2$ m; the mass is set $m_p = 10$ kg; the initial inertia matrix is $J_p = \mathrm{diag}\{10, 10, 10\}$ kg·m^2. To show the effectiveness of the proposed adaptive control, the mass and inertia matrix of the target are respectively assumed to be $m_t = 10$ kg, and

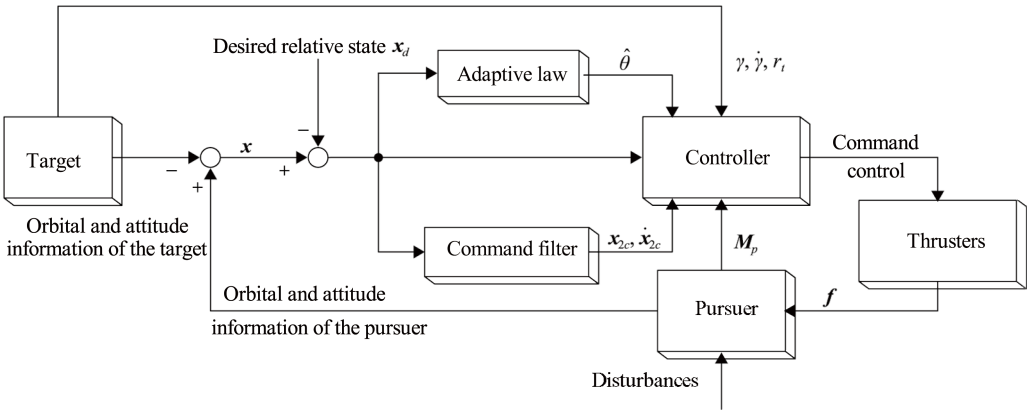

Fig. 3 Structure of the closed-loop system

$$J_t = \begin{bmatrix} 10 & 2.5 & 3.5 \\ 2.5 & 10 & 4.5 \\ 3.5 & 4.5 & 10 \end{bmatrix} \text{ kg·m}^2.$$

For relative information between the pursuer spacecraft and target, the initial relative position, velocity, attitude, and angular velocity are respectively set as

$$\boldsymbol{p}(0) = \begin{bmatrix} 10 & -10 & 10 \end{bmatrix}^{\mathrm{T}} \text{ m}$$

$$\boldsymbol{v}(0) = \begin{bmatrix} 5 & -4 & 4 \end{bmatrix}^{\mathrm{T}} \text{ m/s}$$

$$\boldsymbol{q}(0) = \begin{bmatrix} 0.3772 & -0.4329 & 0.6645 & 0.4783 \end{bmatrix}^{\mathrm{T}}$$

$$\omega(0) = \begin{bmatrix} 0 & 0 & 0 \end{bmatrix}^{\mathrm{T}} \text{ rad/s}.$$

According to [27], the disturbance forces $\boldsymbol{F}_d$ and torques τ_d in (15) can be lumped as

$$\boldsymbol{F}_d = \boldsymbol{F}_{d0} + \boldsymbol{F}_{ds}\sin(\omega_t t) + \boldsymbol{F}_{dc}\cos(\omega_t t) \text{ N}$$

$$\tau_d = \tau_{d0} + \tau_{ds}\sin(\omega_t t) + \tau_{dc}\cos(\omega_t t) \text{ N·m}.$$

Suppose that

$$\boldsymbol{F}_{d0} = \begin{bmatrix} 0.05 & 0.01 & 0.04 \end{bmatrix}^{\mathrm{T}}, \boldsymbol{F}_{ds} = \begin{bmatrix} 0.1 & 0.2 & 0.03 \end{bmatrix}^{\mathrm{T}},$$

$$\boldsymbol{F}_{dc} = \begin{bmatrix} 0.02 & 0.08 & 0.04 \end{bmatrix}^{\mathrm{T}}, \tau_{d0} = \begin{bmatrix} 2 & 1 & 3 \end{bmatrix}^{\mathrm{T}} \times 10^{-3},$$

$$\tau_{ds} = \begin{bmatrix} 1 & 2 & 3 \end{bmatrix}^{\mathrm{T}} \times 10^{-3}, \tau_{dc} = \begin{bmatrix} 2 & 3 & 1 \end{bmatrix}^{\mathrm{T}} \times 10^{-3}.$$

Taking the integrated control law into account, we choose $k = 0.15$, $k_q = k_\theta = 1$, $k_h = 1 \times 10^6$; then, to ensure the condition (45) holds, set $\alpha = 0.5$, $\beta = 1$. Consequently, for any $\omega_n \geqslant 4$, the condition (45) will be satisfied. As for the command filter (31), let $\zeta = 1/\sqrt{2}$ and respectively select $\omega_n = 4, 10, 50$ to observe the influence of the command filter parameter ω_n on the system response.

Figs. 4–7 show the relative position and attitude maneuvers with the command filter parameter $\omega_n = 4$, 10, 50, respectively. Figs. 8 and 9 illustrate the thrust histories with the corresponding ω_n. From the simulation results, it can be seen that fast and precise relative position and attitude control is achieved for the current system, in spite of external disturbances and unknown system parameters. These figures also show that the variations of the system states perform similar with different ω_n except for first several seconds, which reflects that the tracking ability of the command filter is nearly the same fast when $\omega_n \geqslant 4$. In other words, the parameter $\omega_n \geqslant 4$ is able to guarantee the high bandwidth of the command filter such that the output of the filter can fast track the states $\boldsymbol{x}_{2c}^0$ and $\dot{\boldsymbol{x}}_{2c}^0$, as the tracking error curves show in Fig. 10. However, Figs. 8–9 state that the control input varies greatly when ω_n changes. Larger value of the parameter ω_n requires more control power, which would need higher requirement for the propulsion system, especially the maximum thrust. Specifically, as can be seen from Figs. 8 and 9, when $\omega_n = 4$, thrusters with the maximum force 30 N may be satisfying; while for $\omega_n = 50$, thrusters should afford maximum power nearly 360 N, which will result in higher payloads and other difficulties. Hence, based on the considerations of both control input and system performances, a small value of ω_n satisfying the condition (45) may be preferable in practice.

Figs. 11 and 12 illustrate the variations of estimate vector $\hat{\theta}$ and estimate error $\tilde{\theta}$ for the case $\omega_n = 4$. As

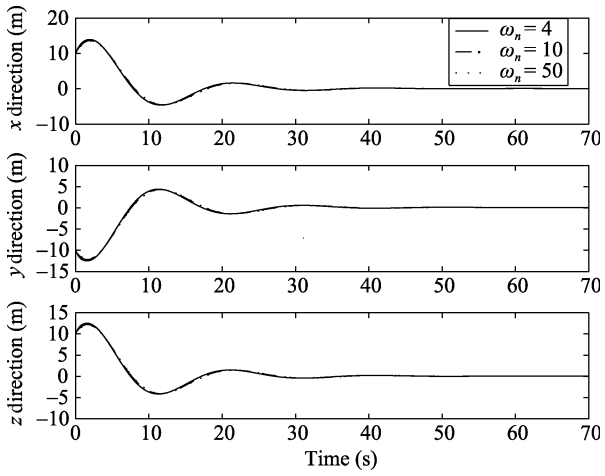

Fig. 4 Relative position

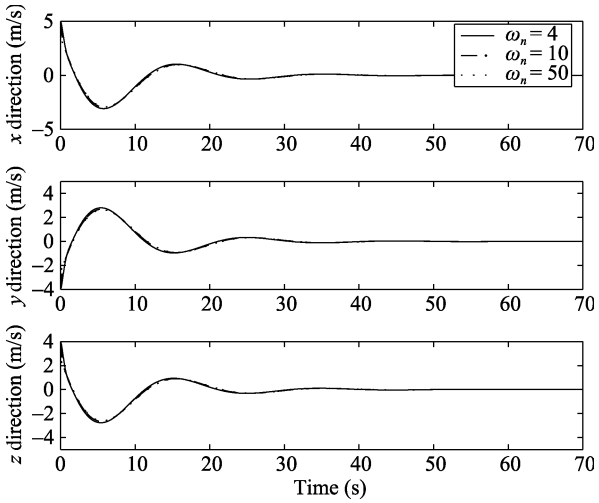

Fig. 5 Relative velocity

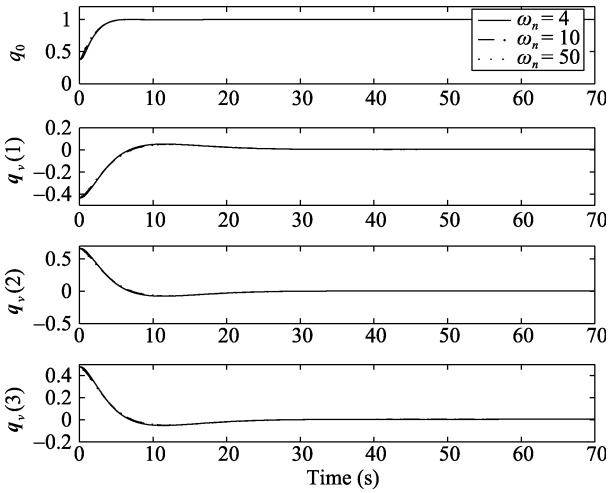

Fig. 6 Relative attitude quaternion

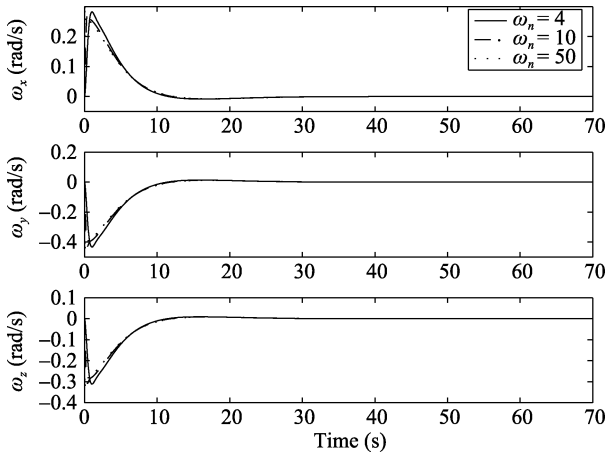

Fig. 7 Relative angular velocity

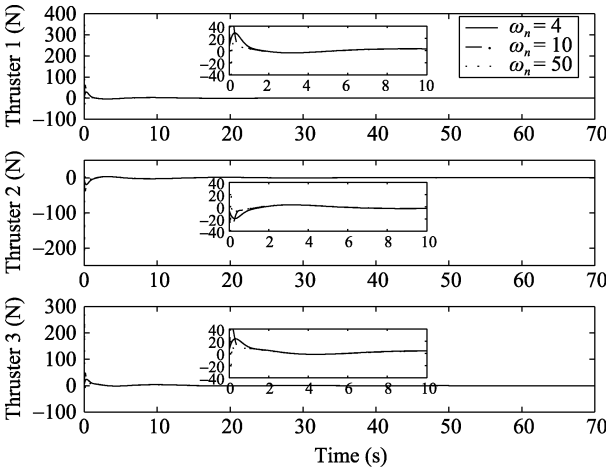

Fig. 8 Control thrusts 1−3

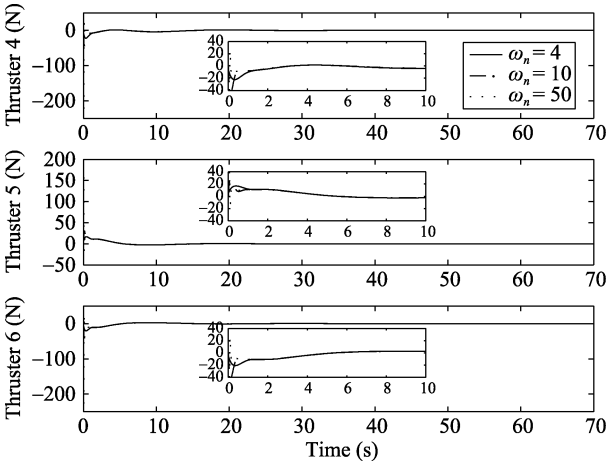

Fig. 9 Control thrusts 4−6

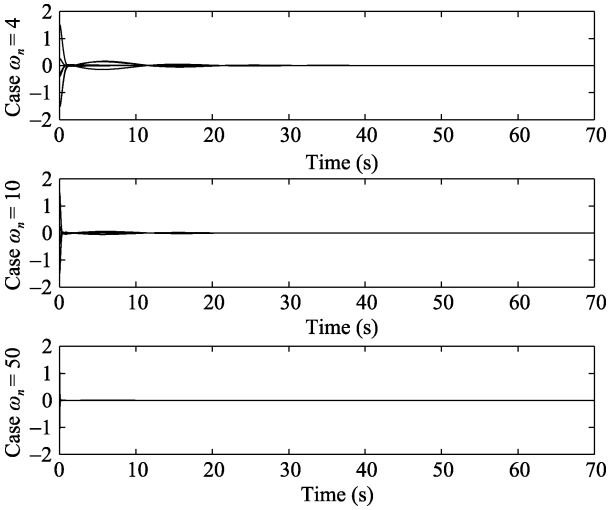

Fig. 10 Command tracking error $\boldsymbol{x}_{2c}^{0} - \boldsymbol{x}_{2c}$

figures depict, with the effect of the adaption law (47), the components of the estimate $\hat{\theta}$ converge to a neighborhood of

zero, and meanwhile the components of the estimate error $\tilde{\theta}$ are bounded. Nevertheless, the estimated parameters do not converge to their true value, which is mainly due to sufficient frequency components in the tracked states are not guaranteed, i.e., the persistent excitation (PE) condition is not satisfied[28].

Another important thing should be noted is the selection of design parameters. According to Theorem 1, the parameters k_q, α, β, ζ can be first chosen with small values to make the condition (45) easily satisfied. The selection of the parameters k and ω_n should not only ensure the condition (45) to hold, but also takes into account that: 1) the filter parameter ω_n could guarantee enough tracking ability of the command filter; 2) the gain parameter k can be adjusted to guarantee a higher control accuracy according to (61). Subsequently, a large value of k_h and a proper k_θ can be set to get a small ultimate bound of system states due to (61) and meanwhile adjust the dynamical response of the estimate vector $\hat{\theta}$.

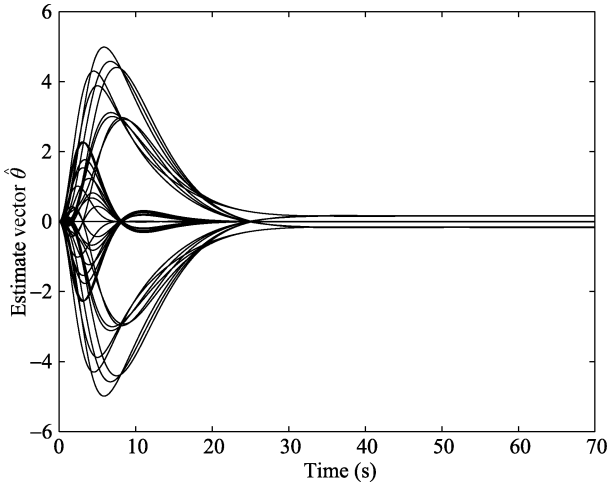

Fig. 11 Estimate vector $\hat{\theta}$

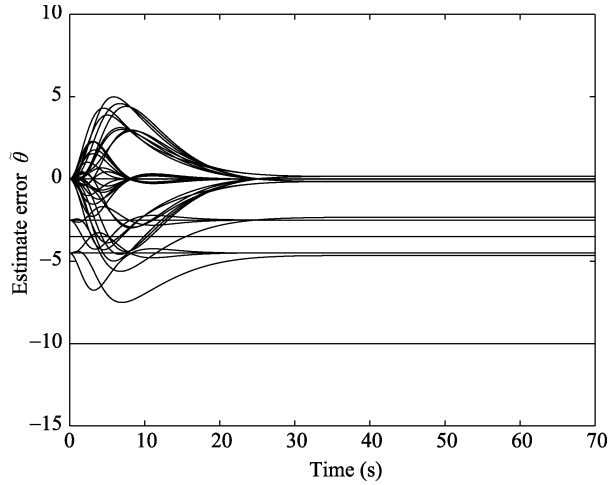

Fig. 12 Estimate error $\tilde{\theta}$

5 Conclusion

In this study, a command filter-based adaptive backstepping control law is developed to deal with the relative translation and attitude motion of a spacecraft in space proximity operation missions. Based on the 6-DOF coupled translational and rotational dynamics of pursuer spacecraft relative to the target[21], using backstepping-based adaptive technology and singular perturbation theory, an integrated position and attitude control strategy is designed, where a command filter is introduced to overcome the "explosion of terms". Within the Lyapunov framework, the proposed control strategy is proved to guarantee ultimate boundedness of the relative position and attitude signals, in spite of bounded disturbances and unknown system parameters; moreover, the corresponding bounds can be made arbitrarily small by adjusting parameters appropriately. The numerical simulation illustrates the effect of the proposed control law; meanwhile, the influence of the command filter parameter on the system is discussed in detail as well.

References

[1] T. E. Rumford. Demonstration of autonomous rendezvous technology (DART) project summary. In *Proceedings of SPIE*, SPIE, Bellingham, USA, vol. 5088, pp. 10–19, 2003.

[2] P. Bodin, R. Larsson, F. Nilsson, C. Chasset, R. Noteborn, M. Nylund. PRISMA: An in-orbit test bed for guidance, navigation, and control experiments. *Journal of Spacecraft and Rockets*, vol. 46, no. 3, pp. 615–623, 2009.

[3] L. Tarabini, J. Gil, F. Gandia, M. A. Molina, J. M. DelCura, G. Ortega. Ground guided CX-OLEV rendezvous with uncooperative geostationary satellite. *Acta Astronautica*, vol. 61, no. 1–6, pp. 312–325, 2007.

[4] P. K. C. Wang, F. Y. Hadaegh. Formation flying of multiple spacecraft with autonomous rendezvous and docking capability. *IET Control Theory & Application*, vol. 1, no. 2, pp. 494–504, 2007.

[5] D. Fragopoulos, M. Innocenti. Autonomous spacecraft 6DOF relative motion control using quaternions and H-infinity methods. In *Proceedings of AIAA, Guidance, Navigation and Control Conference*, San Diego, USA, pp. 1–12, 1996.

[6] P. K. C. Wang, F. Y. Hadaegh, K. Lau. Synchronized formation rotation and attitude control of multiple free-flying spacecraft. *Journal of Guidance Control and Dynamics*, vol. 22, no. 1, pp. 28–35, 1999.

[7] H. Wong, H. Z. Pan, V. Kapila. Output feedback control for spacecraft formation flying with coupled translation and attitude dynamics. In *Proceedings of American Control Conference*, IEEE, Portland, USA, vol. 4, pp. 2419–2426, 2005.

[8] H. Pan, V. Kapila. Adaptive nonlinear control for spacecraft formation flying with coupled translational and attitude dynamics. In *Proceedings of the 40th IEEE Conference on Decision and Control*, IEEE, Orlando, USA, vol. 3, pp. 2057–2062, 2001.

[9] M. Xin, S. N. Balakrishnan, D. T. Stansbery. Spacecraft position and attitude control with $\theta - D$ technique. In *Proceedings of the 42nd AIAA Aerospace Sciences Meeting and Exhibit Renosn*, Reno, USA, AIAA 2004–540, 2004.

[10] M. Xin, H. Pan. Integrated control of position, attitude, and flexible motion for satellite proximity operations. In *Proceedings of AIAA Guidance, Navigation, and Control Conference*, Chicago, USA, AIAA–5670, 2009.

[11] M. Xin, H. Pan. Integrated nonlinear optimal control of spacecraft in proximity operations. *International Journal of Control*, vol. 83, no. 2, pp. 347–363, 2010.

[12] Y. Xu, A. Tatsch, N. G. Fitz-Coy. Chattering free sliding mode control for a 6 DOF formation flying mission. In *Proceedings of AIAA Guidance, Navigation, and Control Conference and Exhibit*, San Francisco, USA, AIAA 2005–6464, 2005.

[13] R. Kristiansen, P. J. Nicklasson, J. T. Gravdahl. Spacecraft coordination control in 6DOF: Integrator backstepping vs passivity-based control. *Automatica*, vol. 44, no. 11, pp. 2896–2901, 2008.

[14] B. B. Sharma, I. N. Kar. Contraction theory-based recursive design of stabilising controller for a class of non-linear systems. *IET Control Theory & Applications*, vol. 4, no. 6, pp. 1005–1018, 2010.

[15] W. S. Chen, J. M. Li. Adaptive output-feedback regulation for nonlinear delayed systems using neural network. *International Journal of Automation and Computing*, vol. 5, no. 1, pp. 103–108, 2008.

[16] D. Swaroop, J. K. Hedrick, P. P. Yip, J. C. Gerdes. Dynamic surface control for a class of nonlinear systems. *IEEE Transactions on Automatic Control*, vol. 45, no. 10, pp. 1893–1899, 2000.

[17] S. J. Yoo, J. B. Park, Y. H. Choi. Adaptive dynamic surface control for stabilization of parametric strict-feedback nonlinear systems with unknown time delays. *IEEE Transactions on Automatic Control*, vol. 52, no. 12, pp. 2360–2365, 2007.

[18] X. Y. Luo, Z. H. Zhu, X. P. Guan. Adaptive fuzzy dynamic surface control for uncertain nonlinear systems. *International Journal of Automation and Computing*, vol. 6, no. 4, pp. 385–390, 2009.

[19] M. Z. Hou, G. R. Duan. Adaptive dynamic surface control for integrated missile guidance and autopilot. *International Journal of Automation and Computing*, vol. 8, no. 1, pp. 122–127, 2011.

[20] J. A. Farrell, M. Polycarpou, M. Sharma, W. Dong. Command filtered backstepping. *IEEE Transactions on Automatic Control*, vol. 54, no. 6, pp. 1391–1395, 2009.

[21] R. Kristiansen, E. I. Grøtli, P. J. Nicklasson, J. T. Gravdahl. A model of relative translation and rotation in leader follower spacecraft formations. *Modeling, Identification and Control*, vol. 28, no. 1, pp. 3–14, 2007.

[22] W. Hahn. *Theory and Application of Liapunov's Direct Method*, New York, USA: Prentice-Hall, 1963.

[23] H. K. Khalil. *Nonlinear Systems*, 3rd ed., Upper Saddle River, USA: Pearson Education, 2002.

[24] O. Egeland, J. T. Gravdahl. *Modeling and Simulation for Automatic Control*, Trondheim, Norway: Marine Cybernetics, 2002.

[25] B. Wie, C. M. Roithmayr. Attitude and orbit control of a very large geostationary solar power satellite. *Journal of Guidance Control and Dynamics*, vol. 28, no. 3, pp. 439–451, 2005.

[26] A. Chaillet, A. Loria. Uniform semiglobal practical asymptotic stability for non-autonomous cascaded systems and applications. *Automatica*, vol. 44, no. 2, pp. 337–347, 2008.

[27] K. Subbarao, S. Welsh. Nonlinear control of motion synchronization for satellite proximity operations. *Journal of Guidance, Control and Dynamics*, vol. 31, no. 5, pp. 1284–1294, 2008.

[28] K. J. Astrom, B. Wittenmark. *Adaptive Control*, 2nd ed., New York, USA: Addison-Wesley Publishing Company, 1995.

Feng Zhang received the M. Sc. degree from the School of Astronauts, Harbin Institute of Technology, China in 2009. He is currently a Ph. D. candidate in Harbin Institute of Technology.

His research interests include spacecraft guidance and control, and nonlinear control.

E-mail: jimmyzf2004@gmail.com (Corresponding author)

Guang-Ren Duan received his Ph. D. degree in control systems theory in 1989 from Harbin Institute of Technology, China. From 1989 to 1991, he was a postdoctoral researcher at Harbin Institute of Technology, where he became a professor of control systems theory in 1991. He visited the University of Hull, UK, and the University of Sheffield, UK from December 1996 to October 1998 and worked at the Queen's University of Belfast, UK from October 1998 to October 2002. Since August 2000, he has been elected specially employed professor at Harbin Institute of Technology sponsored by the Cheung Kong Scholars Program of the Chinese government. He is currently the director of the Center for Control Systems and Guidance Technology at Harbin Institute of Technology. He is a chartered engineer in the UK, a senior member of IEEE and a fellow of IEE.

His research interests include robust control, eigenstructure assignment, descriptor systems, missile autopilot design, and magnetic bearing control.

E-mail: g.r.duan@hit.edu.cn